ChemPubSoc Europe

DOI: 10.1002/cbic.201800167

CHEMBIOCHEM Full Papers

VIP *Very Important Paper*

SPECIAL ISSUE

The Photophysics of Polythiophene Nanoparticles for Biological Applications

Ilaria Bargigia,[a] Elena Zucchetti,[a, b] Ajay Ram Srimath Kandada,[a] Miguel Moreira,[c] Caterina Bossio,[a] Walter P. D. Wong,[d] Paulo Barbeitas Miranda,[a, b, e] Paolo Decuzzi,[c] Cesare Soci,[d] Cosimo D'Andrea,[a, b] and Guglielmo Lanzani*[a, b]

In this work the photophysics of poly(3-hexylthiophene) nanoparticles (NPs) is investigated in the context of their biological applications. The NPs, made as colloidal suspensions in aqueous buffers, present a distinct absorption band in the low-energy region. On the basis of systematic analysis of absorption and transient absorption (TA) spectra taken under different pH conditions, this band is associated with charge-transfer states generated by the polarization of loosely bound polymer chains and originating from complexes formed with electron-withdrawing species. Importantly, the ground-state depletion of these states upon photoexcitation is active even on microsecond timescales, thus suggesting that they act as precursor states for long-living polarons; this could be beneficial for cellular stimulation. Preliminary transient absorption microscopy results for NPs internalized within the cells reveal the presence of long-living species, further substantiating their relevance in biointerfaces.

Introduction

The presence of a π-conjugated carbon skeleton, much akin to many biomolecules, makes conjugated organic polymers potentially viable materials for biological applications.[1] They have been already successfully implemented in electrolyte gated transistors,[2,3] electrodes, ionic devices,[4] sensors,[5–8] and optical interfaces.[9–13] In particular, thin films of poly(3-hexylthiophene) (P3HT) have been employed as optical interfaces to trigger cellular activity upon photoexcitation.[14,15] This capability even enabled neuronal stimulation and subsequent creation of implants that restored vision in blind rats.[16] Although the interfaces in these scenarios are extended surfaces over millimeter-length scales, the scaling down of such interfaces to smaller particles should bring advantages such as easy delivery and closer interaction with cells and organelles: characteristics that enhance and extend the range of possible applications. Moreover, colloidal suspensions of NPs of hundreds of nanometers in dimensions can easily be fabricated, particularly in aqueous solutions,[17,18] thus making them biocompatible.[18–21] In fact, the biocompatibility of P3HT NPs has already been established, as well as the possibility of using them as bio-organic interfaces both for sensing and as actuators.[22] In particular, through suitable modulation of their dimension and surface properties (e.g., surface net charge),[23,24] they can easily pass through the plasma membrane and become internalized in cells both in vitro and in vivo. P3HT NPs have been shown to be photoactive in hydrae, a simple fresh water polyp species, in which they induce different contraction behavior in the animal and affect RNA transcription.[25] These results suggest a photoinduced interaction between the P3HT NPs and the animal cells, though the exact coupling mechanism is still unknown.

Despite much promising evidence of the potential of P3HT NPs for biological applications, a thorough photophysical characterization is still lacking, especially with regard to the nature of the elementary photoexcitations and their dynamics in the NPs when in contact with water and ionic species.[26–29] This hampers a full understanding of their biological effects and phototransduction mechanism, which remains a challenge.

In this work we have employed transient and steady-state photomodulation spectroscopy techniques to identify the elementary excitations in the NPs and to investigate their excited-state dynamics. The study has been extended to water-based buffers at different pH values and to NPs inside living cells.

[a] *Dr. I. Bargigia, Dr. E. Zucchetti, Dr. A. R. S. Kandada, Dr. C. Bossio, Prof. P. B. Miranda, Prof. C. D'Andrea, Prof. G. Lanzani*
Center for Nano Science and Technology @Polimi
Istituto Italiano di Tecnologia
via Pascoli 70/3, 20133 Milano (Italy)
E-mail: guglielmo.lanzani@iit.it

[b] *Dr. E. Zucchetti, Prof. P. B. Miranda, Prof. C. D'Andrea, Prof. G. Lanzani*
Department of Physics, Politecnico di Milano
Piazza Leonardo da Vinci 32, 20133 Milano (Italy)

[c] *Dr. M. Moreira, Dr. P. Decuzzi*
Laboratory of Nanotechnology for Precision Medicine
Istituto Italiano di Tecnologia
via Morego 30, 16163 Genova (Italy)

[d] *Dr. W. P. D. Wong, Prof. C. Soci*
School of Material Science and Engineering
Nanyang Technological University
Singapore 637371 (Singapore)

[e] *Prof. P. B. Miranda*
São Carlos Physics Institute, University of São Paulo
CP 369, Sao Carlos, SP 13560-970 (Brazil)

Supporting information and the ORCID identification numbers for the authors of this article can be found under: https://doi.org/10.1002/cbic.201800167.

This article is part of a Special Issue on Biosensing and Bioimaging.

Results and Discussion

The ground-state (GS) absorption spectrum of P3HT NPs suspended in ultrapure water is shown in Figure 1 A. According to a few earlier works,[30,31] the high-energy part of the spectrum is associated with disordered chains, whereas π-stacked aggregates mainly contribute to the low-energy region. By using the model of weakly interacting H-aggregates developed by Spano

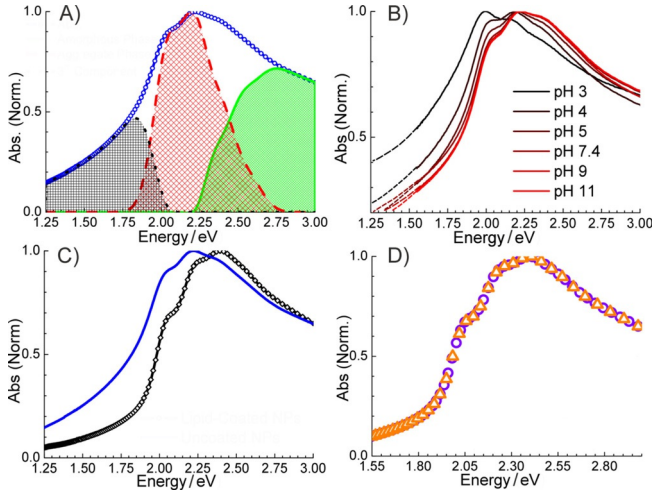

Figure 1. A) GS absorption spectrum of P3HT NPs in ultrapure water (○). ——: amorphous part. -----: aggregate part (see text). ····: third component peaking around 1.83 eV. B) GS absorption of P3HT NPs in buffered solutions at different pH values. C) Absorption spectrum of coated lipid-PEG-P3HT NPs (◇) in comparison with that of uncoated NPs (——). D) Ground-state absorption spectrum of coated lipid-PEG-P3HT NPs in KRH at pH 3 (○) and 7.4 (△).

and co-workers[30,31] it is possible to extract its spectral components. The amorphous phase has a broad featureless absorption band, due to inhomogeneous broadening of intra-chain absorption. The aggregate phase shows a more structured absorption band, assigned to a weakly interacting exciton transition coupled to vibronic states. From the model, we can estimate that the percentage of aggregates[30] in the NPs is ≈24% and that the free exciton bandwidth of the aggregates is $W=$ 33 meV, which corresponds to an intermolecular excitonic coupling (J_{inter}) of ≈8 meV.[32] However, a third component at low energy, not usually reported in literature,[26] is needed to reconstruct the experimentally measured absorption spectrum fully (dotted line). From the difference between the experimental data and the sum of the amorphous and the aggregate phases we see that this component peaks around 1.8 eV and that it extends considerably towards the near infrared. Notably, it is usually absent or negligible in thin films.[30,33]

Indications as to the nature of the low-energy tail are provided by measurements of NPs suspended in ion-rich buffers. We used the Krebs–Ringer-HEPES (KRH) buffer, which is usually adopted as an extracellular medium for electrophysiology measurements and characterized by an ionic activity matching that in the cytosol of cells. It is composed of NaCl, KCl, CaCl, MgCl, $NaCO_2$, HEPES, and D-glucose. Samples of NPs in KRH buffers of pH values ranging from pH 11 to 3 are prepared, and their corresponding absorption spectra are shown in Figure 1 B. Because protons tend to polarize the polymer, this observation suggests that the low-energy states are caused by a distribution of charge-transfer (CT) states, generated either by the polarization of the polymer chains or, somewhat equivalently, by the protonation of the polymer backbone inducing a change in the chain polarizability.

Further evidence is provided by the absorption spectrum of NPs coated with a lipid-PEG corona (for details see the Supporting Information) and suspended in pure water (Figure 1 C). The absorption edge of the coated NPs is sharper, due to the suppression of the low-energy tail. The action of the protons should be greater at the surface of the NP, where the chains are more exposed to the buffer. Accordingly, in the NPs with a lipid-PEG corona the change in the absorption spectrum upon changing the pH does not occur (Figure 1 D). We thus conjecture that proton penetration is responsible for the observed spectral changes, that the lipid-PEG shell halts this, and that the chains responsible for these states are, for the majority, loosely bound chains protruding from the surface into the solvent.

Steady-state photoluminescence (PL) measurements show that the shape of the PL spectrum is insensitive to pH variations (Figure S1 in the Supporting Information): whereas CT states are mainly non-radiative, PL originates from radiative states insensitive to pH.

Figure 2 A shows transient differential transmission ($\Delta T/T$) spectra of the NPs in ultrapure water (pump energy 2.38 eV, pump-probe time delays of 5 ps, 900 ps, and 100 ns).

The positive signal from 1.66 to 2.63 eV is ground-state bleaching (GSB), whereas the negative signal is photoinduced absorption (PA) attributed to hole polarons.[29,34] This band is still present after 900 ps, unlike in thin films of pristine polymer, in which case the PA band is already extinguished after 400 ps.[35] In the same figure we show the spectra of the third spectral component and of the aggregate phase identified in Figure 1 A. The latter spectrum is normalized to the peak of the GSB signal at 5 ps. The GSB extends more towards lower energies than the exciton bleaching contribution and, remarkably, the region of the third spectral component corresponds to a bleach signal, thus ruling out the possibility of it originating exclusively from the contribution of scattering. A change in the real part of the dielectric function could in principle change the scattering efficiency, yet the observed signal is far too large to be due to such an effect.

Going from 5 ps (squares) to 100 ns (triangles), there is a decrease in the peak at 2.2 eV and a red shift of the GSB. Dynamics taken at 2.21 and 1.91 eV are reported in Figure 2 B for delay times up to 1 ns and in Figure 2 C for delays up to 400 ns. Data are normalized to the initial peak. The pump at 2.4 eV excites both the amorphous and the aggregate phases. From the GSB spectral shape, however, we can infer that bleaching of the amorphous phase is negligibly small, perhaps due to an ultrafast energy transfer to the aggregate phase. Furthermore, the transient spectrum clearly shows that a fraction of the excitation involves the states in the tail of the absorption; dynamics support this picture. Higher-energy fea-

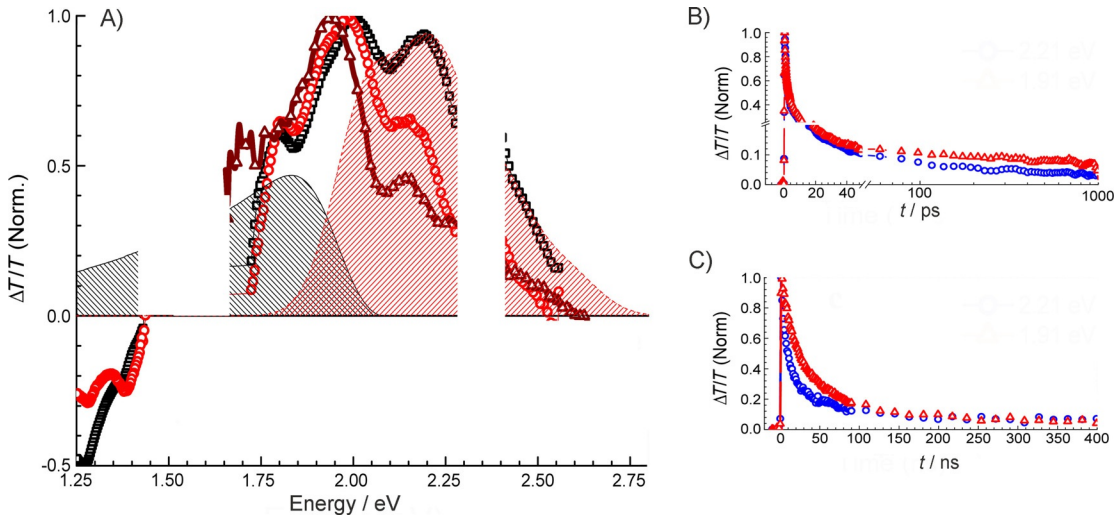

Figure 2. A) $\Delta T/T$ spectra of NPs in pure water at pump-probe time delays of 5 ps (□), 900 ps (○), and 100 ns (△); also reported are the spectra of the aggregate phase (····) normalized to the GSB at 2.24 eV–5 ps time delay and of the third component (——). B) Dynamics at 2.21 eV (○) and 1.19 eV (△) for pump-probe delays up to 1 ns (pump pulse duration ≈200 fs). C) Dynamics at 2.21 (○) and 1.91 eV (△) for pump-probe delays up to 400 ns (pump pulse duration ≈700 ps).

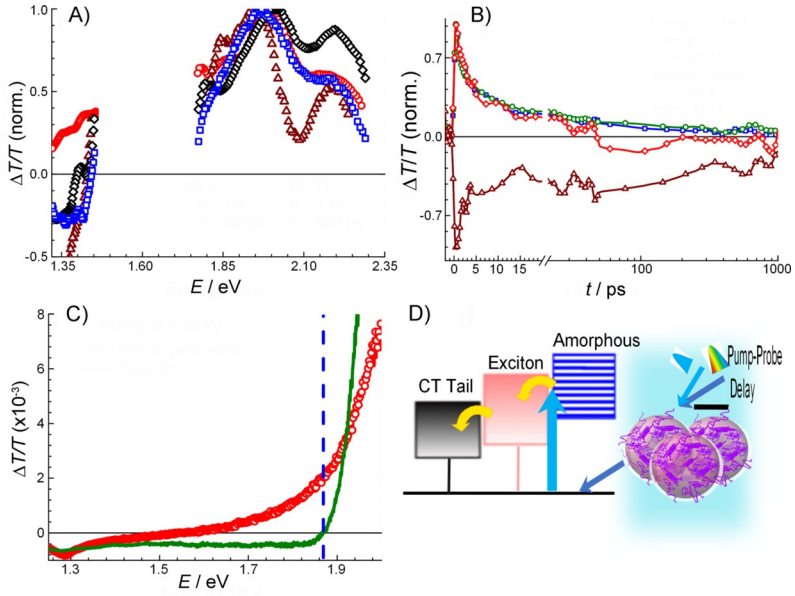

Figure 3. A) $\Delta T/T$ spectra of P3HT NPs in KRH at 1 and 900 ps for pH 11 (◇ and □, respectively) and for pH 3 (○ and △, respectively). B) Dynamics at 2.21 and 1.35 eV for both pH 11 (○ and △, respectively) and pH 3 (□ and ◇, respectively). C) CW PIA spectra of P3HT NPs in pure water (○) and of a cast thin film of P3HT (——) with the pump at 2.33 eV. D) Schematic of the photoexcitation pathway.

tures decay faster than lower-energy ones, showing a red shift of the GSB band even within the first nanosecond. Moreover, the GS depletion, notably in the tail of the spectrum, is not fully recovered even for the longest time range. From Figure 3B we can estimate that after 1 ns ≈3–5% of the initial population has not yet decayed to the GS. With such a long delay, we think that the transient GSB spectrum is an almost pure signature of the low-energy state distribution because singlet states should have been deactivated earlier.[22] The long lifetime of the low-energy region is particularly interesting in view of the application of these NPs as bio-organic interfaces, for an ultrafast recombination rate under continuous wave (CW) light photoexcitation would hardly lead to any significant population of photoexcited species that could lead to efficient communication with cells.

Pump-probe data for the NPs in ion-buffered solutions at pH 11 and at pH 3 are compared in Figure 3. Figure 3A shows the spectra at delays of 1 ps and 900 ps, whereas Figure 3B shows the time decay traces at 2.21 and 1.35 eV for both pH values. The transient spectrum at pH 11 is similar to the one obtained for ultrapure water (Figure 1A), with the GSB in the 1.85–2.5 eV region and the PA signal of polarons from 1.45 to 1.25 eV. Under acidic conditions (pH 3), however, the GSB undergoes a red shift and overwhelms the PA, extending towards

low energies. At long time delays, the PA signature below 1.45 eV is recovered as in the pH neutral solution, because even though the PA contribution is reduced by recombination, it overwhelms the GSB from the tail states at these long timescales. These results suggest spectral migration of the photoexcitation energy to the low-energy tail. Because the low-energy tail is more prominent at low pH, the positive signal becomes dominant. We conjecture that the states in the tail are complexes formed with electron-withdrawing species (oxygen, hydrated oxygen, protons) that behave as precursors for charge generation. Note that assignment of the absorption tail (Figure 1 A) to polarons, possibly formed by polymer oxidation,[36,37] does not explain the transient absorption (TA) data, for in this case pump-probe spectra would hardly show the long-lived bleaching in the same region. In Figure 3 D we report a schematic of what we believe to be the photoexcitation pathway.

Finally, continuous wave photoinduced absorption (CW-PIA) data also show a bleaching signal, up to 1.6 eV (Figure 3 C). This indicates that photoexcitation generates states with lifetimes exceeding the millisecond time domain. GSB in the long-wavelength region corresponds to the depletion of the broad distribution of CT states that are assigned here to the protonation of the polymer chain. Notably, the extended bleaching is a distinct characteristic of the nanoparticles, for it does not appear in the CW PIA spectrum of the thin film (Figure 3 C, ——).

To probe NPs that are in contact with living cells locally, with ultrafast time resolution, we built a transient-absorption microscopy[38] setup (a schematic is shown in Figure 4, right). This requires singling out of a small signal out of a large fluctuating background. Results were obtained by pumping at 2.37 eV and probing at 2.18 eV (Figure 4), which provides information on the bleaching recovery. The initial decay of the GSB signal, in the 1–100 ps time domain, is much faster in cells than in suspension, whereas the long-lived tail is still present and comparable to that in suspension. The initial fast decay kinetics can be attributed to the increase in the non-radiative decay rate due to additional energy dissipation paths provided by the environment. The mechanism could be ultrafast vibrational redistribution and vibrational cooling leading to heating of the cytoplasm, although electronic energy transfer to unidentified acceptors in the corona surrounding the NPs or acceptors distributed within the cytoplasm cannot be excluded. Similar behavior was recently observed in time-resolved photoluminescence measurements performed on the same NPs in cells.[22] Decay of the GSB signal implies fast GS population recovery, thus ruling out charge-transfer reactions. The long-lived tail, however, seems to indicate that even in cells there are long-lived states, perhaps those that we identify as charge-transfer states, that are precursors for charge generation and might support photocatalytic activity.

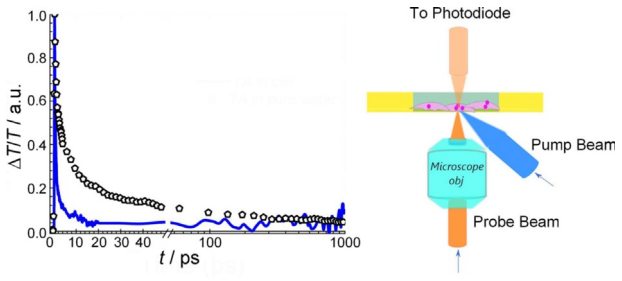

Figure 4. Left. Solid line: $\Delta T/T$ dynamics (2.18 eV) of NPs internalized within a living cell (——) and in pure water (○). Right) Schematic of the transient absorption microscopy setup.

Conclusion

We have investigated the excited-state dynamics of P3HT NPs in different media relevant to biology, including the cell membrane, by transient and steady-state photomodulation spectroscopy. We have found that the photoexcitation dynamics in NPs are different from those in the solid state (e.g., thin film), highlighting the role of the volume/surface area ratio and of the morphology, both of which are affected by the shape and the size of the aggregates. In the ground-state absorption spectrum the NPs show low-energy features that we attribute to a distribution of CT states generated by the polarization of the loosely bound polymer chains that protrude into the solvent. Accordingly, their electronic structure is very sensitive to pH changes in the buffer: in particular, low pH values enhance the charge generation efficiency. Encapsulation of the NPs in a protective lipid-PEG corona impedes formation of these states in the suspension; however, this is totally ineffective once the NP is internalized because during the endocytosis process the PEG corona is lost (as shown by time-resolved photoluminescence data, Figure S2). The results in cells support the hypothesis that there is a photocatalytic action upon photoexcitation in vivo, showing the existence of a population of long-lived states that we assign to charge carriers. If it is assumed that the NP ($R > 100$ nm) totally absorbs CW radiation at 2 eV with 1 mW mm^{-2} with the subsequent generation of a fraction of 0.1 % of carriers with lifetime of 1 ms, the estimated steady-state number of long-lived charges per NP is 100. This number is certainly enough for supporting photocatalytic activity in the cell and a non-negligible biological reaction, while being below the toxicity threshold as observed in the experiments.[22] Our results suggest a way to engineer NP characteristics—in terms of morphological properties, for example—to enhance the long-lived population yield upon photoexcitation and to boost its impact for biological applications.

Experimental Section

TA spectroscopy and microscopy

fs-TA setup: A Coherent Micra Ti:Sapph oscillator and a Coherent RegA 9040 amplifier were used to perform TA measurements up to 1 ns time delay (pump pulse duration ≈200 fs, 250 KHz). Probe light transmitted through the sample was collected with an imaging spectrometer (Acton SP2300i) coupled to a custom silicon-based CCD linear array (Stresing camera). An energy density of ≈10–30 μJ cm^{-2} was used to excite the NPs in suspension in a cuvette of 1 mm pathlength (typical spot diameter of the pump beam ≈500 μm, estimated at the $1/e^2$ plane).

fs-setup for microscopy: We used the same laser as described above. The probe beam was focused with a 20× objective (Zeiss, NA 0.22) onto NPs internalized into cells (Figure 4, right). The pump beam was overlapped onto the probe beam passing outside of the objective. Transmitted probe beam was collected with a 10× objective (Melles Griot, NA 0.25) and sent to a Si photodiode. The signal from the photodiode was sent to a lock-in amplifier (Stanford Research Systems, reference frequency ≈787.7 Hz) and computer-processed to yield $\Delta T/T$ data. Typical pump fluence used was ≈20–80 $\mu J\,cm^{-2}$ (typical beam diameter at $1/e^2$ plane was ≈30 μm).

ns-setup: The pump beam was provided by a Q-switched Nd:YVO_4 laser (Innolas Picolo), electronically triggered and synchronized to a fs Ti:Sapph laser (Quantronix Integra-C, pulses ≈100 fs, 1 KHz repetition rate), used to generate a broadband white light probe beam by focusing the fundamental pulses at 800 nm into a thin sapphire plate. With the jitter taken into account, the system has a time resolution of approximately 1 ns. Detection was provided by a monochromator coupled to a Si photodiode. Typical spot diameter of the pump ≈297 μm at the $1/e^2$ plane, typical pump power used 3.2 mW.

CW-PIA spectroscopy: CW-PIA spectra were recorded under CW laser excitation (532 nm, ≈100 mW, beam diameter 6 mm), probing the induced change in transmission ($\Delta T/T$) with a broadband FTIR spectrometer (Bruker Vertex 80v) equipped with a Si detector. P3HT NPs in solution were kept in home-built CaF_2 cuvettes and measured in transmission configuration. A long-pass filter (580 nm) was used to prevent aliasing and damage to the detector due to stray scattered laser light. The differential signal of over 2000 consecutive scans with pump light on and off was averaged (i.e., $\Delta T/T = T_{on} - T_{off}/T_{off}$) to increase the signal-to-noise ratio.

Sample preparation for fs-TA microscopy: HEK-293 cells in their culture medium and with small amounts of NPs were washed three times with pure water and the culture medium was substituted with KRH prior to measurements. For more details, please refer to the Supporting Information.

Acknowledgements

P.B.M. acknowledges a visiting scholarship (BPE) from Fundação de Amparo à Pesquisa do Estado de São Paulo (FAPESP) (Brazil).

Conflict of Interest

The authors declare no conflict of interest.

Keywords: biological applications · conjugated polymers · nanoparticles · photophysics · ultrafast spectroscopy

[1] G. Lanzani, *Nat. Mater.* **2014**, *13*, 775.
[2] T. Cramer, A. Campana, F. Leonardi, S. Casalini, A. Kyndiah, M. Murgia, F. Biscarini, *J. Mater. Chem. B* **2013**, *1*, 3728.
[3] D. Khodagholy, J. Rivnay, M. Sessolo, M. Gurfinkel, P. Leleux, L. H. Jimison, E. Stavrinidou, T. Herve, S. Sanaur, R. M. Owens, G. G. Malliaras, *Nat. Commun.* **2013**, *4*, 2133.
[4] J. Isaksson, P. Kjäll, D. Nilsson, N. D. Robinson, M. Berggren, A. Richter-Dahlfors, *Nat. Mater.* **2007**, *6*, 673.
[5] L. Torsi, G. M. Farinola, F. Marinelli, M. C. Tanese, O. H. Omar, L. Valli, F. Babudri, F. Palmisano, P. G. Zambonin, F. Naso, *Nat. Mater.* **2008**, *7*, 412.
[6] M. A. C. Stuart, W. T. S. Huck, J. Genzer, M. Müller, C. Ober, M. Stamm, G. B. Sukhorukov, I. Szleifer, V. V. Tsukruk, M. Urban, F. Winnik, S. Zauscher, I. Luzinov, S. Minko, *Nat. Mater.* **2010**, *9*, 101.
[7] J. Rivnay, R. M. Owens, G. G. Malliaras, *Chem. Mater.* **2014**, *26*, 679.
[8] C. Wu, B. Bull, K. Christensen, J. McNeill, *Angew. Chem. Int. Ed.* **2009**, *48*, 2741; *Angew. Chem.* **2009**, *121*, 2779.
[9] V. Benfenati, N. Martino, M. R. Antognazza, A. Pistone, S. Toffanin, S. Ferroni, G. Lanzani, M. Muccini, *Adv. Healthcare Mater.* **2014**, *3*, 392.
[10] V. Gautam, D. Rand, Y. Hanein, K. S. Narayan, *Adv. Mater.* **2014**, *26*, 1751.
[11] D. Ghezzi, M. R. Antognazza, R. Maccarone, S. Bellani, E. Lanzarini, N. Martino, M. Mete, G. Pertile, S. Bisti, G. Lanzani, F. Benfenati, *Nat. Photonics* **2013**, *7*, 400.
[12] D. Ghezzi, M. R. Antognazza, M. Dal Maschio, E. Lanzarini, F. Benfenati, G. Lanzani, *Nat. Commun.* **2011**, *2*, 166.
[13] M. R. Antognazza, N. Martino, D. Ghezzi, P. Feyen, E. Colombo, D. Endeman, F. Benfenati, G. Lanzani, *Adv. Mater.* **2014**, *26*, 7662.
[14] N. Martino, P. Feyen, M. Porro, C. Bossio, E. Zucchetti, D. Ghezzi, F. Benfenati, G. Lanzani, M. R. Antognazza, *Sci. Rep.* **2015**, *5*, 8911.
[15] P. Feyen, E. Colombo, D. Endeman, M. Nova, L. Laudato, N. Martino, M. R. Antognazza, G. Lanzani, F. Benfenati, D. Ghezzi, *Sci. Rep.* **2016**, *6*, 22718.
[16] J. F. Maya-Vetencourt, D. Ghezzi, M. R. Antognazza, E. Colombo, M. Mete, P. Feyen, A. Desii, A. Buschiazzo, M. Di Paolo, S. Di Marco, F. Ticconi, L. Emionite, D. Shmal, C. Marini, I. Donelli, G. Freddi, R. Maccarone, S. Bisti, G. Sambuceti, G. Pertile, G. Lanzani, F. Benfenati, *Nat. Mater.* **2017**, *16*, 681.
[17] H. Shimizu, M. Yamada, R. Wada, M. Okabe, *Polym. J.* **2008**, *40*, 33.
[18] D. Tuncel, H. V. Demir, *Nanoscale* **2010**, *2*, 484.
[19] C. Wu, B. Bull, C. Szymanski, K. Christensen, J. McNeill, *ACS Nano* **2008**, *2*, 2415.
[20] M. Peters, N. Zaquen, L. D'Olieslaeger, H. Bové, D. Vanderzande, N. Hellings, T. Junkers, A. Ethirajan, *Biomacromolecules* **2016**, *17*, 2562–2571.
[21] L. Feng, C. Zhu, H. Yuan, L. Liu, F. Lv, S. Wang, *Chem. Soc. Rev.* **2013**, *42*, 6620.
[22] E. Zucchetti, M. Zangoli, I. Bargigia, C. Bossio, F. Di Maria, G. Barbarella, C. D'Andrea, G. Lanzani, M. R. Antognazza, *J. Mater. Chem. B* **2017**, *5*, 565–574.
[23] C. He, Y. Hu, L. Yin, C. Tang, C. Yin, *Biomaterials* **2010**, *31*, 3657.
[24] A. Verma, F. Stellacci, *Small* **2010**, *6*, 12.
[25] C. Tortiglione, M. R. Antognazza, A. Tino, C. Bossio, V. Marchesano, A. Bauduin, M. Zangoli, S. V. Morata, G. Lanzani, *Sci. Adv.* **2017**, *3*, e1601699.
[26] S. N. Clafton, D. M. Huang, W. R. Massey, T. W. Kee, *J. Phys. Chem. B* **2013**, *117*, 4626.
[27] J. A. Labastide, M. Baghgar, I. Dujovne, B. H. Venkatraman, D. C. Ramsdell, D. Venkataraman, M. D. Barnes, *J. Phys. Chem. Lett.* **2011**, *2*, 2089.
[28] Z. Hu, D. Tenery, M. S. Bonner, A. J. Gesquiere, *J. Lumin.* **2010**, *130*, 771.
[29] K. N. Schwarz, S. B. Farley, T. A. Smith, K. P. Ghiggino, *Nanoscale* **2015**, *7*, 19899.
[30] J. Clark, J. F. Chang, F. C. Spano, R. H. Friend, C. Silva, *Appl. Phys. Lett.* **2009**, *94*, 2007.
[31] J. Clark, C. Silva, R. H. Friend, F. C. Spano, *Phys. Rev. Lett.* **2007**, *98*, 1.
[32] F. C. Spano, *J. Chem. Phys.* **2005**, *122*, 234701.
[33] N. Banerji, S. Cowan, E. Vauthey, A. J. Heeger, *J. Phys. Chem. C* **2011**, *115*, 9726.
[34] J. Piris, T. E. Dykstra, A. A. Bakulin, P. H. M. Van Loosdrecht, W. Knulst, M. T. Trinh, J. M. Schins, L. D. A. Siebbeles, *J. Phys. Chem. C* **2009**, *113*, 14500.
[35] A. R. S. Kandada, G. Grancini, A. Petrozza, S. Perissinotto, D. Fazzi, S. S. K. Raavi, G. Lanzani, *Sci. Rep.* **2013**, *3*, 2073.
[36] L. Romaner, T. Piok, C. Gadermaier, R. Guentner, P. Scandiucci de Freitas, U. Scherf, G. Cerullo, G. Lanzani, E. J. W. List, *Synth. Met.* **2003**, *139*, 851.
[37] C. Gadermaier, L. Romaner, T. Piok, E. J. W. List, B. Souharce, U. Scherf, G. Cerullo, G. Lanzani, *Phys. Rev. B* **2005**, *72*, 1.
[38] T. Chen, F. Lu, A. M. Streets, P. Fei, J. Quan, Y. Huang, *Nanoscale* **2013**, *5*, 4701.

Manuscript received: March 28, 2018
Accepted manuscript online: May 1, 2018
Version of record online: June 25, 2018